Single-phase Resonant DC Link Inverter with integrated isolation for PV generators.

S. Foti[1*], S. De Caro[1], A. Oteri[1], T. Scimone[2], A. Testa[1]
[1]D.I. University of Messina, sfoti@unime.it, (*Italy*)
[2]D.I.E.E.I. University of Catania, tommaso.scimone@unict.it, (*Italy*)

2023 International Conference on Clean Electrical Power (ICCEP) | 979-8-3503-4837-8/23/$31.00 ©2023 IEEE | DOI: 10.1109/ICCEP57914.2023.10247373

***Abstract*— A single phase resonant DC link inverter is proposed in this paper for the connection of domestic Photo-Voltaic or solid state Thermo-Electric generators to the AC grid. High efficiency is obtained thanks to a single-stage configuration and a resonant dc link structure providing low switching power losses, furthermore, a high frequency transformer integrated into the resonant dc link leads to a full exploitation of the input dc voltage and to the achievement of some typical features of two-stage inverters, such as voltage step-up, isolation, and very low leakage current. The high switching frequency made possible by soft switching finally leads to smaller and more efficient output filters. The consistence of the proposed configuration is assessed through the simulation of a 6kW PV plant.**

***Index Terms* — Grid tied inverter, PV generators, Thermo-Electric generators, Resonant DC Link, Single-Stage power conversion, HF Transformer.**

I. INTRODUCTION

Voltage source PWM inverters are by far the most popular solution for connecting to the ac grid electric generators featuring a dc output, such as those based on Photo-Voltaic (PV) power or Thermo-Electric Generators (TEG). PV systems are today widely diffused in distributed generation a domestic level, while solid state TEG based on the Seebeck effect are a promising technology for recovering the waste everywhere a sufficient temperature difference exists in the industrial, transportation and domestic sectors. The structure inverters designed to equip these systems is generally more complex than that of inverters for electric motors drives, having to reach specific goals, such as very high efficiency levels over a wide range of working conditions, high reliability, prevention of unwanted islanding operations, suppression of high frequency leakage currents, and very low direct current fed into the grid. Inverter for small PV or TEG plants are characterized by the number of power processing stages, provision for input/output isolation, and the type of isolation transformer if any [1]. Hard switching inverters (HSI) are the most common choice, because of circuit simplicity and rugged control schemes. The simplest HSI configuration for small electricity generators is composed of a PWM dc/ac converter, which is fed by the PV or TEG array and delivers power to the grid. A low-pass output filter is essential to obtain a good THD. Although advantaged by a low-cost and high peak efficiency such a single stage configuration is burdened by some key disadvantages, because being tasked not only to inject a sinusoidal current into the grid but, at the same time, of Maximum Power Point Tracking (MPPT) and, if required, of voltage amplification. Furthermore, the absence of an internal isolation leads to the introduction of a low frequency transformer on the grid side, or of special measures to prevent the circulation of high frequency leakage currents and the injection of dc current into the grid as well. Most of inverters for grid connected small electric generators feature a two-stage structure [2]-[6], where, as shown in Fig. 1, the dc/ac converter is supplemented by a dc/dc one. The latter performs the MPPT and voltage amplification, freeing of these tasks the dc/ac converter, and accomplishing them with greater efficiency. Moreover, a very compact high frequency isolation transformer can be integrated into the dc/dc converter. As a result, dual-stage inverters provide a high efficiency on a wider operating range, however featuring a greater complexity and higher cost.

The basic structure of the single-phase dc/ac converter present in both single and dual-stage inverter configurations is based on an H4 bridge topology, as shown in Figure 1.

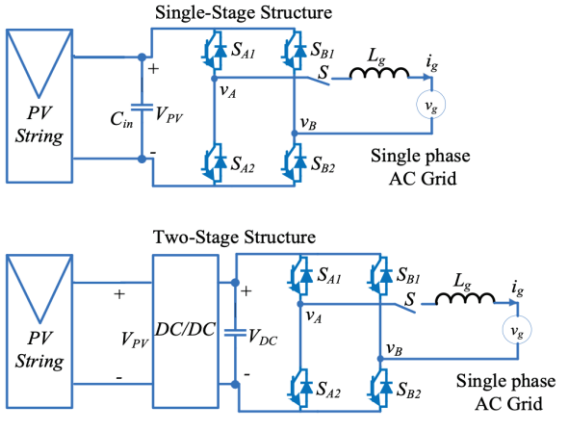

Fig. 1 Single (up) and dual stage (down) inverter configurations.

More complex single-phase inverter structures are those based on H5, H4 with DC-Bypass, H4 with Zero Voltage Rectifier, HERIC or multilevel topologies [7]-[14]. Their switching frequencies are usually below *20 kHz*, because higher switching frequencies, which would be desirable to achieve higher power density by making smaller the magnetic components, are in practice prevented on HSI by unacceptable switching power losses and EMI issues. As an answer, Soft Switching Inverters (SSI) have been developed [15]-

[19], which achieve a considerable reduction of the switching power losses through Zero-Voltage Switching (ZVS) or Zero-Current Switching (ZCS) operations, obtained with the introduction of one or more resonant cells [20]. Among SSI, Resonant DC Link (RDCL) inverters have been proposed as a mean for increasing the switching frequency, leading to reduction of the size and power losses of transformers, output low pass filters and other reactive components of the inverter. The basic concept of the RDCL inverter was developed in the 80s [21],[22] and recently proposed for grid connected inverters [23],[24]. The basic structure of a RDCL inverter is shown in Figure 2. A resonant cell, formed by L_r and C_r, produces a DC-Link voltage V_{DC} oscillating at some tens or hundreds of kHz. Since V_{DC} features a sinusoidal oscillation, it becomes periodically null, providing the grounds for ZVS operations of the four inverter switches, achieving very low switching power losses. A key drawback of such a kind of inverter is the huge peak reached by the oscillating voltage, which causes on the power devices a voltage stress greater than twice the dc input voltage. A possible solution to this issue is provided by the Active-Clamped Resonant DC Link (AC-RDCL) configuration [25],[26]. As shown in Figure 3, an additional power device S_r is used to clamp the dc link voltage at a preset value reducing the voltage stress on power devices. However, the active clamping worsens the utilization of the dc bus voltage.

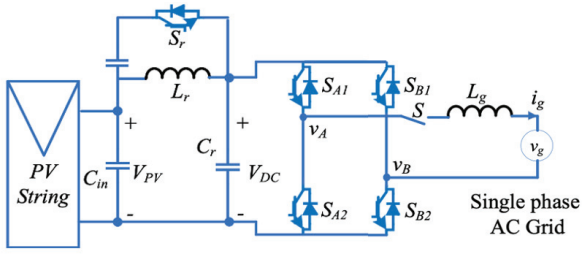

Fig. 2 Actively Clamped Resonant DC-Link Inverter.

A single-stage, single-phase Resonant DC Link (RDCL) inverter is proposed in this work, providing characteristics which are typically found in two-stage configurations, such as input-output isolation, voltage step-up, compact output filter, and very low leakage current. Such an RDCL inverter is obtained by adding a High-Frequency (HF) transformer and a single power switch to the conventional RDCL configuration. The HF transformer enables the change of the voltage conversion ratio through turns ratio variation, compensating for input voltage variations. This is a quite important feature for inverters equipping domestic PV plants as it enables a compensation of the PV array output voltage drift with irradiation level and temperature. In a typical domestic PV system, only a few turns ratio changes are required during a daily operating cycle, which can be achieved using cheap relays. Furthermore, the HF transformer prevents the circulation of high-frequency leakage currents when using three-level unipolar PWM techniques, leading to smaller and more efficient output filters.

II. THE PROPOSED RDCL INVERTER TOPOLOGY

As shown in Fig. 3, the proposed RDCL inverter is formed of a resonant LC tank, a transformer, and a H-bridge dc/ac converter. Compared to the conventional RDCL inverter topology, a transformer is introduced providing input/output insulation and voltage boosting. The L_r, C_r, cell provides a high frequency oscillating voltage V_{TR1}, which is stepped up by the transformer, generating a sinusoidal secondary voltage $V_{TR2}=nV_{TR1}$. Some taps are present on the primary winding to enable the turns ratio n to take two values, $n_a=N_{1a}/N_2$ and $n_b=N_{1b}/N_2$. Turns ratio variation is accomplished by means of electromagnetic or solid-state relays to face the drift of the PV array output voltage. Moreover, an idle condition N_0 is introduced, for the system start-up.

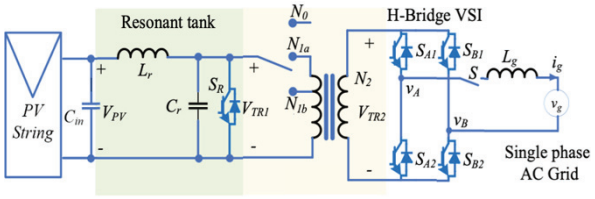

Fig. 3 The proposed RDCL Inverter.

The sinusoidal secondary voltage V_{TR2} goes null periodically, thus enabling the inverter switches (S_{A1}, S_{A2}, S_{B1}, and S_{B2}) to switch at zero voltage, leading to a dramatic reduction of switching power losses. Figure 4 deals with an equivalent circuit of the proposed RDCL inverter. A current generator replaces the transformer and bridge converter, while the LC cell stray resistance is accounted through R_s. This in practice coincides with the inner resistance of the inductor, because of the negligible equivalent series resistance of ceramic and polyester capacitors.

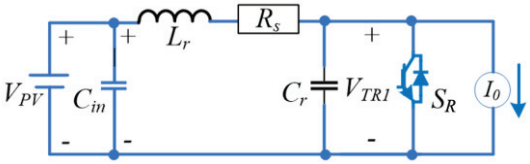

Fig. 4 Equivalent circuit of the RDCL inverter.

A resonant cell is characterized by the resonance angular frequency ω_0 and characteristic inductance Z_0, which are given by:

$$\omega_0 = \frac{1}{\sqrt{L_r C_r}} \qquad Z_0 = \sqrt{\frac{L_r}{C_r}} \tag{1}$$

An operational cycle of the proposed inverter starts with the switch S_R turned on. The resonant capacitor voltage is null, while the current circulating in the resonant inductance linearly increases, until reaching $I_{Lr}(0)$ when S_R is turned off at $t=0$. This starts the oscillation of the voltage and current within the LC cell. Under the hypothesis that the load current I_0 remains constant throughout a resonance period T_0 and neglecting the stray resistance R_s, the resonant capacitor voltage V_{TR1} and the resonant inductor current I_{Lr} are

given by:

$$V_{TR1}(t) = V_{PV} + \omega_0 L_r A sin(\omega_0 t) - B cos(\omega_0 t) \quad (2)$$

$$I_{Lr}(t) = I_0 + \frac{B}{\omega_0 L_r} sin(\omega_0 t) + A cos(\omega_0 t) \quad (3)$$

where $A = (I_{Lr}(0) - I_0)$ and $B = \left(V_{PV} - V_{TR1}(0)\right)$.

If $V_{TR1}(0)=0$ and $I_{Lr}(0)= I_0$, V_{TR1} and V_{TR2} become zero at $t=k/\omega_0$ ($k = 1, 2, 3, ..., n$), enabling in these instants zero-voltage turn-on of the four inverter switches. Furthermore, the peak value of the resonant capacitor voltage ($\widehat{V_{TR1}}$) reaches $2V_{PV}$ at $t=1.5k/\omega_0$, as shown in Figure 5.

Thanks to ZVS at turn-on, the inverter switching power losses P_{sw} closely matches the turn-off losses:

$$P_{sw} = \frac{I_0^2\, t_f^2}{144\, C_r} f_0 \quad (4)$$

being t_f the fall time and $f_0 = \omega_0/2p$ the resonance frequency.

Conduction losses P_{cond} are given by:

$$P_{cond} = \frac{6 I_0\, V_{on}}{\pi} \quad (5)$$

being V_{on} the on-state voltage of the power devices.

The average inverter input voltage ($\overline{V_{TR2}}$) can be obtained from:

$$\overline{V_{TR2}} = \frac{1}{2}\widehat{V_{TR2}} = \frac{n}{2}\widehat{V_{TR1}} = \frac{n}{2} 2V_{PV} = nV_{PV} \quad (6)$$

Some power losses are caused by the inductor stray resistance, which can be written as a function of inverter output power P_0, inductor quality factor Q, impedance of the resonant link Z_0 and average input voltage $\overline{V_{TR2}}$:

$$P_{ESR} = \frac{1}{Q}\left(\frac{P_0}{\overline{V_{TR2}}}\right)^2 Z_0 + \frac{\overline{V_{TR2}}^2}{2QZ_0} \quad (7)$$

The energy E_W lost during each resonant cycle in the stray resistance R_s is given by:

$$E_W = \frac{R_s}{2} I_0^2\, T_0 = \int_o^{T_0} P_{ESR} dt \quad (8)$$

If not compensated, the loss of energy in the resonant cell causes a gradual decrease of the magnitude of the oscillating voltage V_{TR2}, which no longer returns to zero at the end of each cycle, thus preventing ZVS operation.

To achieve a continuous oscillation, it is necessary to restore the energy E_w lost by the LC cell in each resonant cycle. Hence, the switch S_R is briefly turned on for a time T_{on} at the start of each resonance cycle. Because during T_{on} the load current I_0 exceeds I_{Lr}, the latter gradually increases, thus transferring energy to the resonant inductance. The energy E_L supplied to L_r within a resonance cycle is:

$$E_L = \frac{V_{PV}^2}{2L_r} T_{on}^2 \quad (9)$$

A continuous oscillation is achieved if E_L exacly matches E_W. Figure 6 highlights the importance of the compensation of the energy lost. If the inductor charging at the beginning of each resonant cycle is deactivated, the oscillation of the primary voltage quickly ends.

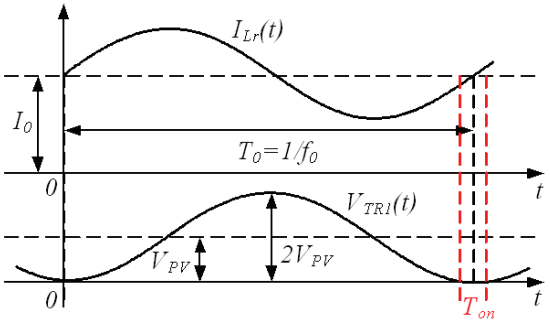

Fig. 5 Operation of the LC cell.

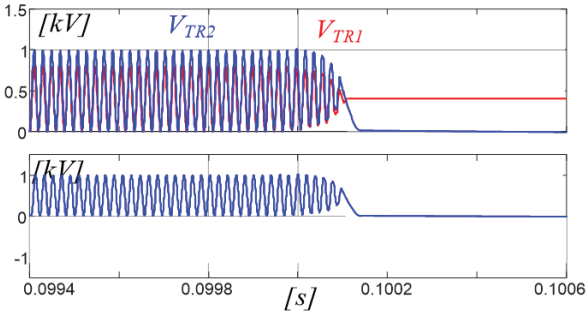

Fig. 6 Deactivation of resonant capacitor charging.

The RDCL inverter total power losses can be computed as composition of switching and conduction losses in the ac/dc converter and resonant LC cell losses:

$$P_{TOT} = P_{SW} + P_{cond} + P_{ESR} \quad (10)$$

It is possible to determine the value of L_r which minimizes the total power losses. From differentiation of the function $P_{TOT}(L_r)$ it comes that the optimal resonant inductance is given by:

$$L_r = \frac{3\overline{V_{TR2}}^2}{f_0 \pi \sqrt{Q\overline{V_{TR2}}^2 \left(I_0^2 t_f^2 f_0^2\right) + 72P_0^2}} \quad (11)$$

The diagram of the function $P_{TOT}(L_r)$, as obtained from data provided in Tabs. I ÷ II, is shown in Fig. 7. The optimal value of L_r, at the maximum power and $\overline{V_{TR2}}$, is *93.7 mH*.

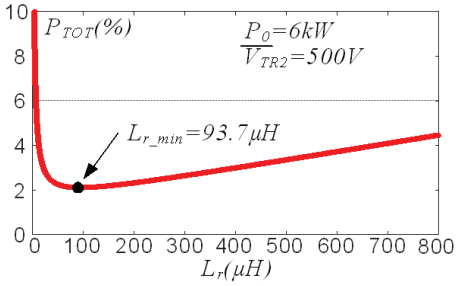

Fig. 7 P_{TOT} vs. L_r.

TABLE I
SYSTEM SPECIFICATIONS

P_0	V_{PV}	$\overline{V_{TR2}}$	I_0
0.25÷6kW	200÷400V	350÷500V	1÷ 26A

TABLE II
IGBT SPECIFICATIONS

Code	V_n	I_n	f_{sw}	V_{cesat}	t_f
STGYA75H120DF2	1200 V	75 A	20kHz	2.1 V	20ns

Based on (1) the resonant capacitance is given by:

$$C_r = \frac{1}{\omega_0^2 L_r} = 0.1\mu F \qquad (12)$$

Because the resonant capacitor is parallel connected to the primary winding of the transformer, the latter should feature a magnetizing reactance at f_0 suitably larger than the capacitive reactance to prevent any effect on LC cell resonant operation, hence the magnetizing inductance L_M must be selected in order to achieve:

$$L_M \gg \frac{1}{\omega_0^2 C_r} = 93.7\mu H \qquad (13)$$

The transformer turns ratio n is another key parameter to be selected to ensure proper operations of the RDCL inverter over the entire range of the PV array output voltage V_{VP}.

In a domestic PV plant, the array output voltage V_{VP} typically varies from 200V to 400V, according to actual values of the irradiation and temperature. Moreover, an input dc voltage of at least 350V is required to enable the inverter to transfer power to a 230V RMS (325V peak) 50 Hz single phase grid. Considering the 200V lower bound of the V_{VP} range, a 0.57 turns ratio is required to achieve a 350V input dc voltage, however this sets a limit to the highest V_{VP} which the inverter can process. In fact, if V_{VP} is larger than 290V, the peak voltage to be withstood by the inverter power switches exceeds 1000V, which is in practice the upper bound of the safe operating area for 1200V IGBT devices. This leads to an unacceptably narrow 200÷290V V_{VP} operating range. On the other hand, to achieve a 1000V dc input voltage with the 400V maximum PV array output voltage, a 0.8 turns ratio is required, which however would require at least 280V to achieve a 350V input dc voltage, leading to a quite unpractical 280÷400V V_{VP} operating range.

To ensure proper operation of the inverter over the entire V_{PV} 200÷400V range a transformer with a tapped primary winding is adopted, which enables an on-line turns ratio variation according to the actual value of V_{PV}. In the proposed system, two possible turns ratios can be selected, namely: $n_a=N_{1a}/N_2=0.57$, for operation with V_{PV} ranging from 200 to 290V, and $n_b=N_{1b}/N_2=0.8$, for operation with V_{PV} ranging from 290 to 400V.

In practice the turn ratio only needs to be changed a handful of times a day, at sunrise, sunset or when cloud shading occurs. This makes it possible to switch from one primary winding tap to another using inexpensive relays.

Transformer parameteters of Table V have been computed by a conventional transformer design approach [5] based on the specifications provided in Table I.

TABLE III
HF TRANSFORMER PARAMETERS

Material	N27	N_2	60
f	50kHz	L_{l1a}	6.2μH
$\overline{V_{TR2}}$	700÷1000V	L_{ma}	21.2mH
$\overline{V_{TR1}}$	400÷800V	L_{l1b}	12 μH
P_n	6kW	L_{mb}	29.4mH
N_{1a}	35	R_{1a}	14.4 mΩ
N_{1b}	48	R_{1b}	20.89 mΩ
R_2	20 mΩ		

III. RDCL INVERTER CONTROL SYSTEM

A suitable control system has been developed to manage the proposed RDCL inverter. As shown in the schemes of Figures 8 an9, it encompasses four main sections, each one providing a specific function.

Voltage modulation is accomplished by exploiting a sigma-delta synchronous approach, which enables ZVS operation and a precise closed loop output voltage control. Such an approach achieves unipolar voltage modulation by dynamically adjusting the density of voltage pulses, as illustrated in Figure 10.

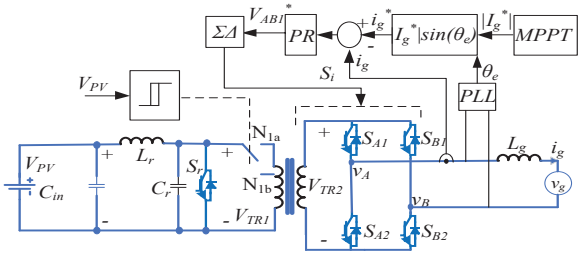

Fig. 8 Scheme of Control system.

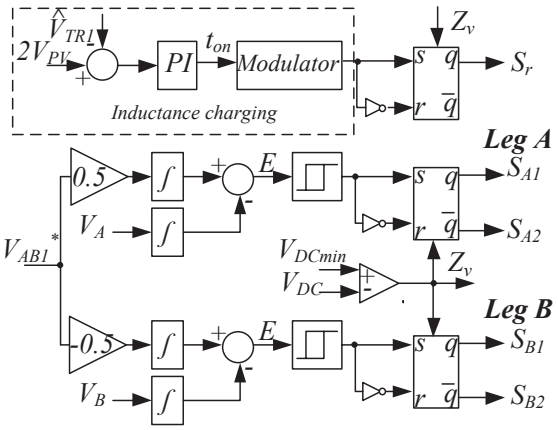

Fig. 9 Sigma-delta modulator with inductance charging.

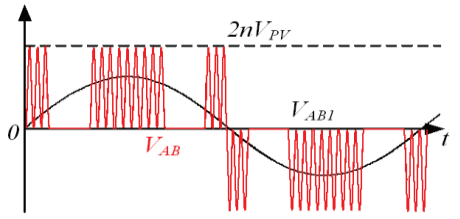

Fig. 10 Output voltage V_{AB} and fundamental component V_{AB1}

Output current control is achieved through a proportional-resonant regulator (PR), providing stable and efficient operation. This regulator achieves zero steady-state error without requiring transformation to a rotating reference system. A Phase Locked Loop (PLL) system is exploited to synchronize the reference output current with the grid voltage.

Resonant inductance charging is managed by acting on the additional switch S_r, which is briefly turned on at the start of each resonant cycle. The on-time T_{on} is determined by a Proportional-Integral (PI) regulator that processes the difference between the actual peak voltage across the resonant capacitor and twice the input DC voltage V_{PV}.

A Maximum Power Point Tracking (MPPT) is crucial to extract at any time the maximum available power from a PV array or a TEG system. An incremental conductance approach is exploited to accomplish the MPPT acting on the active power fed to the grid. This in turn can be controlled by adjusting either the magnitude of the inverter output current or the phase angle (φ) between voltage and current.

The selection of the transformer turns ratio is managed by a hysteretic comparator, which triggers the transition to the proper turns ratio (n_a or n_b) according to the actual value of V_{PV}. Dangerous voltage spikes may occur when changing the turns ratio, due to the energy trapped in the inductive components of the system. These can be prevented by introducing suitable Metal Oxide Varistors (MOV) or by driving to zero the load current for a short time.

IV. Simulations

A *6kW* PV plant is considered to assess the consistence of the proposed configuration by simulation. The PV array if formed of two strings, each one encompassing a series of 13 PV modules (213 W- 60 PV cells). Each module features at *25°C*: V_{oc}=*36.3V*, i_{sc}=*7.84A*, V_{mp}=*29V*, i_{mp}=*7.35A*. The PV array output voltage V_{PV} ranges from *200V* to *400V* with a *377V* MPP voltage at *25°C* and full irradiation. A step up transformer with the parameters shown in Table II is included in the simulated system with two selectable turns ratios (n_a=*0.57*, n_b=*0.8*). An idle condition is also provided for disconnecting the transformer from the resonant tank. The inverter is equipped with four *1200V* IGBT devices, operating at *50kHz*, which is the frequency at which the LC cell resonates. The quality factor Q of the resonant inductor is *200*. The inverter feeds a *230V*, *50Hz* single-phase grid, featuring a *0.1mH* inductance and a *1mΩ* resistance.

A system start-up is shown in Figure 11. At the beginning, the transformer is disconnected from the grid by switching the turns ratio selector to the idle position. The resonant circuit starts to work, and the oscillation of the voltage is controlled through S_R. After a short time, the relay switches to N_{2A} and the power stream towards the grid is established. Steady state operation is described in Fig. 12 and Fig. 13 with P_{PV}= *3kW*, V_{PV}=*400V*, and n=n_a , Figures 14 and 15 deal with steady state operation at V_{PV}=*200V*, with n= n_a.

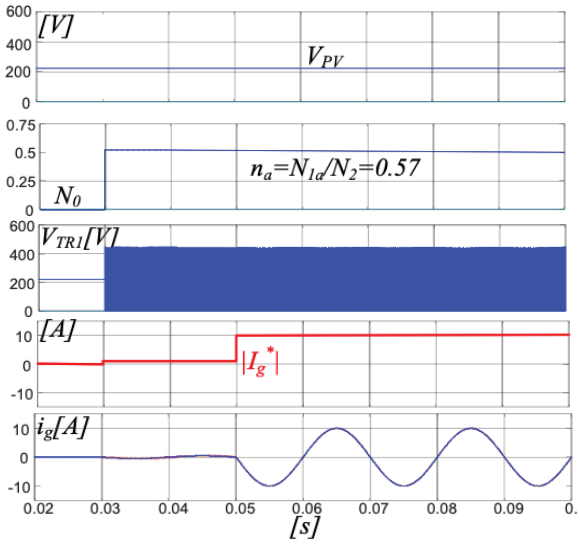

Fig. 11 Inverter start up: V_{PV}, n, Magnitude of the reference load current, V_{TR1}, load current.

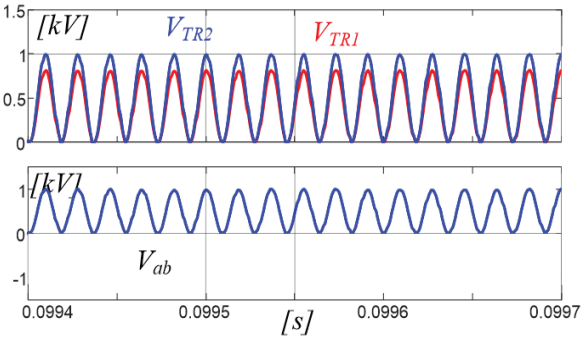

Fig. 12 Steady state, V_{PV}= 400V, n=n_a: V_{TR1}, V_{TR2}, V_{AB}.

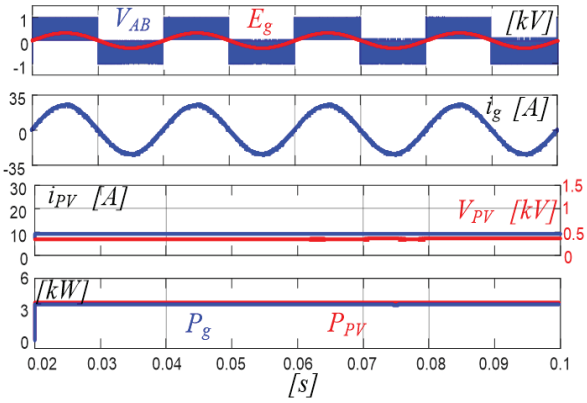

Fig. 13 Steady state, V_{PV}= 400V, n=n_a: V_{AB}, E_g, i_g, V_{PV}, i_{PV}, P_g, P_{PV}.

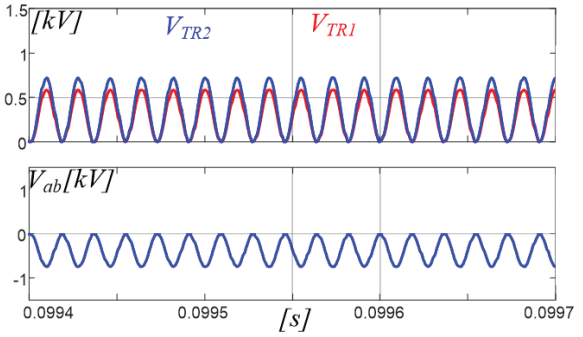

Fig. 14 Steady state: V_{PV}= 200V, n=n_a: V_{TR1}, V_{TR2}, V_{AB}.

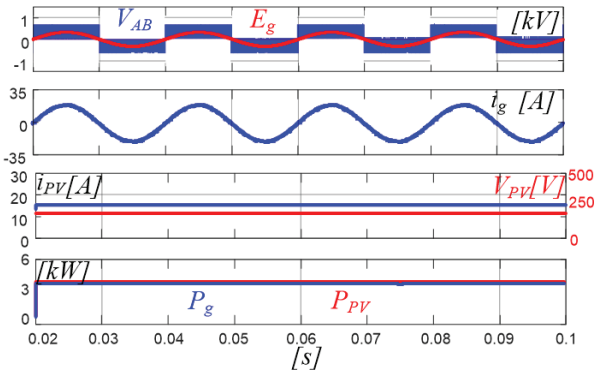

Fig. 15 Steady state: V_{PV}= 200V, n=n_a: V_{AB}, E_g, i_g, V_{PV}, i_{PV}, P_g, P_{PV}.

Fig. 16 deals with operation of the hysteretic comparator which switches the turns ratio from n_a to n_b if V_{PV} rises beyond *290V* or vice-versa, if V_{PV} becomes lower than *280V*. A dangerous voltage spike occurs when changing the turns ratio, due to the trapped inductive energy, leading to the use of a relay with an internal MOV. Voltage spikes can be also prevented by accomplishing the turns ratio change at null load current, as shown in Fig. 17.

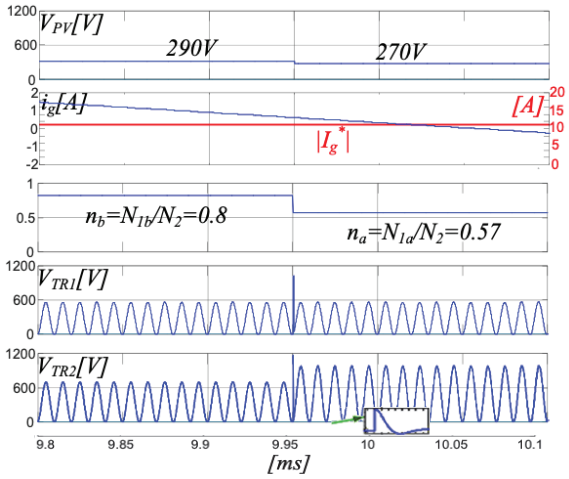

Fig. 16 Overvoltage occurring when switching from n_a to n_b.

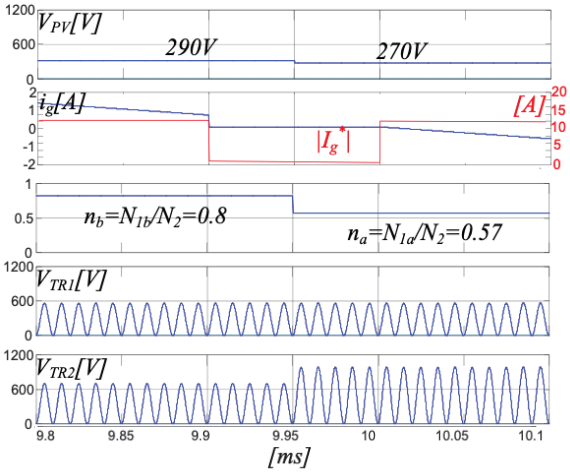

Fig. 17 Zero load current turns ratio switching from n_a to n_b.

MPP operation at *cos(φ)=1* is shown in Fig. 18, while Fig. 19, deals with MPPT operation at *cos(φ)=.9*, highlighting that the proposed configuration is able to manage a reactive power stream, thanks to the reactive components of the resonant circuit. In both cases, as result of a quite precise MPP tracking, the PV array voltage is very close to *377 V*, the MPP PV array voltage at *25°C* and full irradiation. Moreover, a quite reasonable 0.88% grid current THD is obtained.

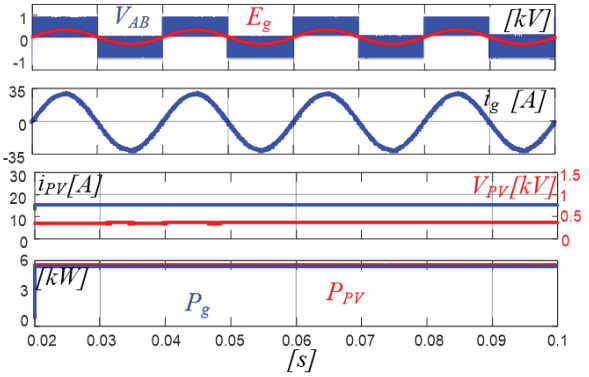

Fig. 18 MPP operation, cos(φ)=1, n=n_b: V_{AB}, E_g, i_g, V_{PV}, i_{PV}, P_g P_P.

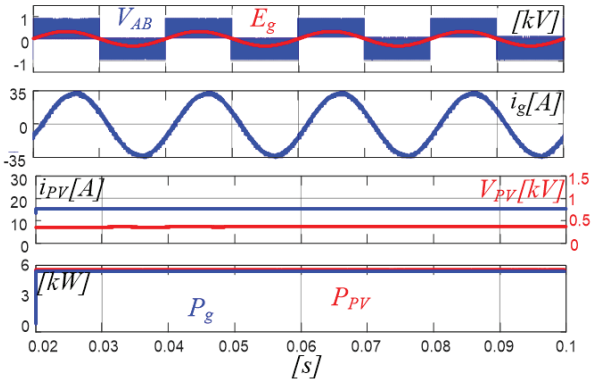

Fig. 19 MPP operation, cos(φ)=0.9, n=n_b: V_{AB}, E_g, i_g, V_{PV}, i_{PV}, P_g P_P.

A comparison with a PV generator of the same power ratings equipped with a non-isolated single-stage PWM inverter operated at *20 kHz* and equipped with the same IGBT devices has been accomplished. Performance comparison is played in terms of the harmonic content of the inverter output voltage and on estimated efficiency.

The THD of the output voltage versus output power is shown in Fig. 20. The proposed configuration achieves a lower THD, mainly due to the higher switching frequency compared to the conventional counterpart. The harmonic spectrum of the grid current achieved by the proposed RDCL inverter at rated load is shown in Fig. 21, fully complying with the limits set by the IEC 61000-3-2 standard on power quality. The proposed inverter performs better than the conventional PWM counterpart also also in terms of power losses according to Fig. 22.

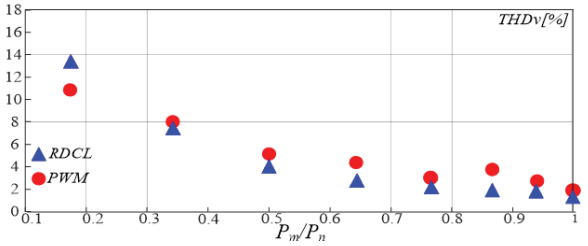

Fig. 20 THD vs. output power.

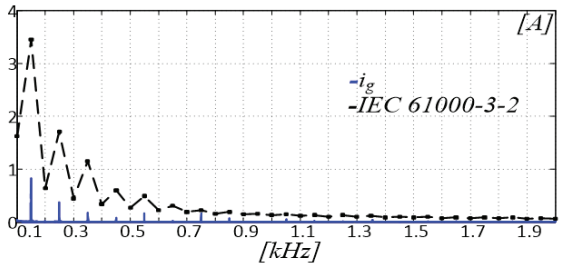

Fig. 21 Spectrum of grid current vs. IEC 61000-3-2 limit.

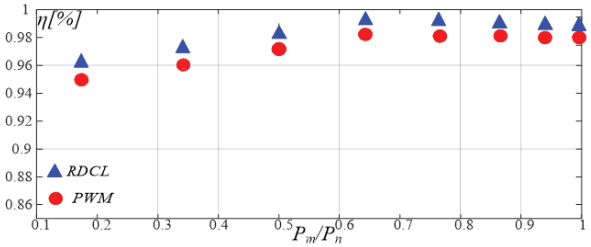

Fig. 22 Efficiency vs. output power.

V. Conclusions

A single-phase resonant DC link inverter for small photovoltaic and TEG plants has been presented featuring an integrated isolation. This is achieved by a HF transformer supplied by the oscillating voltage generated by a LC resonant cell. Tanks to such a transformer, a full exploitation of the input dc voltage is achieved, which is prevented on normal RDCL inverters by the need to clamp the peak of the oscillating voltage. Moreover, the proposed inverter, which is based on a single stage structure, provides characteristics which are typical of two-stage configurations, such as input-output isolation, voltage step-up, compact output filter, and very low leakage current. A transformer with a tapped primary winding enables to change the voltage conversion ratio to compensate for variations of the PV array output voltage with irradiation level and temperature. A *6kW* PV plant has been considered to assess by simulation the consistence of the proposed configuration. The proposed inverter has been shown to perform better in terms of efficiency and output current THD than a standard single-stage PWM inverter for PV applications. Moreover, by increasing the switching frequency up to *50 kHz*, and exploiting unipolar sigma-delta modulation, smaller and more efficient output filters can be adopted compared with the standard inverter operating at *20 kHz*.

Acknowledgment

This work was carried out in the framework of the ARS01_00334 NAUSICA - Program PON «R&I» 2014-2020.

References

[1] S. B. Kjaer, J. K. Pedersen and F. Blaabjerg, "A review of single-phase grid-connected inverters for photovoltaic modules," in IEEE Transactions on Industry Applications, vol. 41, no. 5, pp. 1292-1306, Sept.-Oct. 2005.

[2] Kim J-S, Kwon J-M, Kwon B-H, "High-efficiency two-stage three-level grid-connected photovoltaic inverter", IEEE Trans Ind Electron. 2017, 46 (c), 1.

[3] Barbosa PG, Braga HAC, Barbosa Rodrigues M do Carmo, Teixeira EC, "Boost current multilevel inverter and its application on single-phase grid-connected photovoltaic systems", IEEE Trans Power Electron 2006, 21 (4), pp. 1116–24.

[4] Saha S, Sundarsingh VP, "Novel grid-connected photovoltaic inverter", Proc Inst Electr Eng 1996, 143, (2), pp. 143–56.

[5] Bose BK, Szezesny PM, Steigerwald RL. Microcontroller control of residential photovoltaic power conditioning system. IEEE Trans Ind Appl 1985;21(5):1182–91.

[6] H. Hasabelrasul, Z. Cai, L. Sun, X. Suo and I. Matraji, "Two-Stage Converter Standalone PV-Battery System Based on VSG Control," in *IEEE Access*, vol. 10, pp. 39825-39832, 2022.

[7] G. Rizzoli, et al., "Comparison of single-phase H4, H5, H6 inverters for transformerless photovoltaic applications", IECON, 2016, pp. 3038-3045.

[8] Kibria, M.F.; Elsanabary, A.; Tey, K.S.; Mubin, M.; Mekhilef, S. "A Comparative Review on Single Phase Transformerless Inverter Topologies for Grid-Connected Photovoltaic Systems." Energies 2023, 16, 1363.

[9] W. Yu, J. J. Lai, H. Qian, and C. Hutchens, "High-efficiency MOSFET inverter with H6-type configuration for photovoltaic nonisolated AC-module applications," IEEE Trans. Power Electron., vol. 26, no. 4, pp. 1253–1260, Apr. 2011.

[10] S. Heribert, S. Christoph, and K. Juergen, "HERIC topology," German Patent 10 221 592 A1, Dec. 4, 2003.

[11] T. Kerekes, R. Teodorescu, P. Rodríguez, G. Vázquez, and E. Aldabas, "A new high-efficiency single-phase transformerless PV inverter topology, "IEEE Trans. Ind. Electron., vol. 58, no. 1, pp. 184–191, Jan. 2011.

[12] L. Zhou, F. Gao, and T. Xu, "Implementation of active NPC circuits in transformer-less single-phase inverter with low leakage current," IEEE Trans. Ind. Appl., vol. 53, no. 6, pp. 5658–5667, Nov./Dec. 2017.

[13] S. Foti, T. Scimone, O. Giordano, S. D. Caro and A. Testa, "A Resonant hybrid multilevel inverter," 2022 International Symposium on Power Electronics, Electrical Drives, Automation and Motion (SPEEDAM), 2022, pp. 377-382.

[14] S. Foti, A. Testa, S. De Caro, L. D. Tornello, G. Scelba, M. Cacciato, "Multi-Level Multi-Input Converter for Hybrid Renewable Energy Generators" Energies, 2021, 14, (6), pp. 1764.

[15] Finney, S.J., Green, T.C., and Williams, B.W.: "Review of resonant link topologies for inverters", IEE Proc. B, Vol. 140, No. 2, 1993, pp 103-1 14.

[16] Klassens, J.B., and Smits, E.J.F.M.: "Series resonant ac power interface with an optimal power factor and enhanced conversation ratio", IEEE Trans. Power Electron., July 1988, pp335-343.

[17] T.S. Wu, M. D. Bellar, A. Tchamdjou, J. Mahdavi, and M. Ehsani, "A review of soft-switched DC-AC converters," in Conf. Rec. of IEEE IAS Annual Meeting, 1996, pp. 1133-1144.

[18] M. Mezaroba, D. C. Martins, and I. Barbi, “A ZVS PWM full-bridge inverter with active clamping technique using the reverse recovery energy of the diodes,” in Proc. IEEE 28th Annu. Conf. Ind. Electron. Soc., 2002, vol. 1, pp. 621–626.

[19] Gurunathan and A. K. S. Bhat, “Zero-voltage switching DC link singlephase pulsewidth-modulated voltage source inverter,” IEEE Trans. Power Electron., vol. 22, no. 5, pp. 1610–1618, Sep. 2007

[20] C. Licitra, L. Malesani, G. Spiazzi, P. Tenti and A. Testa, "Single-ended soft-switching electronic ballast with unity power factor," in IEEE Transactions on Industry Applications, vol. 29, no. 2, pp. 382-388, March-April 1993.

[21] D. M. Divan and G. Skibinski, "Zero-switching-loss inverters for high-power applications," in IEEE Transactions on Industry Applications, vol. 25, no. 4, pp. 634-643, July-Aug. 1989.

[22] G. Venkataramanan and D. M. Divan, "Pulse width modulation with resonant DC link converters," Conference Record of the 1990 IEEE Industry Applications Society Annual Meeting, Seattle, WA, USA, 1990, pp. 984-990 vol.2.

[23] Y. Chen, M. Chen and D. Xu, "A 3-kW Two-Stage Transformerless PV Inverter With Resonant DC Link and ZVS-PWM Operation," in *IEEE Transactions on Industry Applications*, vol. 57, no. 2, pp. 1495-1506, March-April 2021.

[24] Y. Chen et al., "A ZVS Grid-Connected Full-Bridge Inverter With a Novel ZVS SPWM Scheme," in IEEE Transactions on Power Electronics, vol. 31, no. 5, pp. 3626-3638, May 2016,

[25] Divan, D.M., and Venkataramarnan, G., and DeDoncker, R.W.A.A.: "Design methodologies for soft switched inverters", IEEE Trans. Ind. Appl. Vo1.29, No.1, 1993, pp 126-135.

[26] Divan, D.M., Malesani, L., Tenti, P., and Toigo, V.: "A synchronised resonant dc link converter for soft-switched PWM", IEEE Trans. Ind. Appl. VO1.29, No.1, 1993, pp 940-948.